Interrelation Between Long-Term Viscoelasticity and Viscoplastic Responses of Semicrystalline Polymers

E. Kontou, G. Spathis

Department of Applied Mathematical and Physical Sciences, Section of Mechanics, National Technical University of Athens, 5 Heroes of Polytechnion, GR-15773, Athens, Greece

Received 28 February 2002; accepted 29 July 2002

ABSTRACT: Two types of linear low-density polyethylenes, prepared by metallocene catalysts were studied experimentally in terms of differential scanning calorimetry, dynamic mechanical analysis (DMA), and tensile testing. The different comonomer content and the small amounts of long branching in one of the materials studied strongly affect the crystalline distribution and morphology and, consequently, the DMA and tensile experimental data. From the experimental DMA data, the function of relaxation modulus, treated as a material property, is used to describe the corresponding tensile experimental results. A constitutive analysis that considers the viscoelastic path at small strains and the viscoplastic one at high strains proved to be capable of describing the tensile behavior of the materials. © 2003 Wiley Periodicals, Inc. J Appl Polym Sci 88: 1942–1950, 2003

Key words: polyethylene; viscoelastic properties; transitions

INTRODUCTION

The prediction of the inelastic mechanical behavior of solid polymers remains an aspect of great importance. A lot of work dealing with the association of yield and postyield behaviors of amorphous glassy polymers with the nonlinear viscoelastic nature of glassy state has been published in recent years.[1–6]

Most of these approaches have treated the nonlinear viscoelasticity in terms of integral representation with multiple relaxation times, stress dependent or with state variables related to the free volume.[7]

In an article by Hasan and Boyce,[8] the nonlinear viscoelastic behavior was modeled as an elastic–inelastic transition, where the energetically distributed nature of inelastic events and their evolution with straining was considered. The model results were compared to the experimental data for true strain rate uniaxial compression tests at different rates and temperatures, whereas the model capability was further tested with compressive creep test at different stresses and temperatures.

An analogous approach[9] based on the development of a unified model, describing both monotonic loading and creep experiments, was recently published. Through this analysis, the rate of plastic deformation in glassy polymers, with a distribution of plastic shear transformations considered, was calculated.

With the assumption of the dominance of a viscoelastic path at small strains, the deformation procedure was treated as a thermally activated one and was described by a constitutive equation of viscoelasticity. Hereafter, the viscoplastic path prevailed, and a decomposition of strain into viscoelastic and viscoplastic parts was applied in terms of a kinematic formulation.

In this study, following analogous ideas, we examined the viscoelastic nature of the deformation mechanism of semicrystalline polymers, up to the yield point and above it, by dynamic mechanical analysis (DMA). Two types of linear low-density polyethylenes (LLDPEs), prepared by metallocene catalysts, were experimentally studied in terms of dynamic mechanical spectroscopy. From the storage modulus versus temperature curves at four different frequencies, the corresponding (apparent) master curves were plotted, and consequently, the relaxation spectra in a logarithmic timescale were evaluated. With these values of relaxation spectra, the relaxation modulus function [$E(t)$] with respect to time was obtained. This function, hereafter, was treated as a material property, able to describe experimental results obtained at a totally different timescale, namely, tensile stress–strain data.

EXPERIMENTAL

Materials

Two types of commercial grade LLDPE, prepared by metallocene catalysts and designated as M_1 and M_2, were studied. Table I summarizes the densities, the melt flow index (MFI) values, and the comonomer

Correspondence to: E. Kontou (eknontou@central.ntua.gr).

Journal of Applied Polymer Science, Vol. 88, 1942–1950 (2003)

TABLE I
Properties of Ethylene Copolymers

Sample type	Density (g/cm^3)	MFI (190°C, 2.16 Kgf)	Comonomer type	Comonomer content (%)
M_1	0.927	3.02	C8	7
M_2	0.926	1.303	C8	9.5

types and amounts used. The density of pellets was measured in an isopropanol–distilled water gradient column calibrated with glass floats. A minimum of four samples was measured to obtain the values given in Table I. The error in the measurement was +0.0002 g/c.

The MFI was measured at 190°C at load of 2.16 Kgf.

The materials were compression molded at 120°C with a thermopress and a special mold of 2 mm in thickness.

Methods

Calorimetric measurements were carried out with a Setaram DSC 141 instrument (Caluire, France) with a pulsed nitrogen cooling system. Both types of materials were treated in the same way: they were heated at a constant heating rate of 40°C/min from ambient temperature up to 150°C to erase previous history. Then, they were held for 2 min at 150°C and subsequently cooled to 0°C at a cooling rate of 20°C/min. After an isothermal hold of 2 min, the samples were heated at a rate of 10°C/min, and the corresponding thermogram was recorded. Calculations of the percentage crystallinity were based on a heat of fusion of 290 J/g for the perfect crystal[10] and are presented in Table II. The melting temperature, heat of fusion, and percentage crystallinity were expected to decrease as the comonomer content inreased.[11] When samples M_1 and M_2 were compared, the effect of comonomer was expressed by the shifting of the melting temperature to a lower value for sample M_2, whereas its heat of fusion was slightly higher, probably due to the inhomogeneous distribution of crystal size and morphology. Sample M_2 was characterized by small amounts of long-chain branching, meaning that it was a substantially linear polyethylene; however, this branching did not affect the density of the material.

DMA experiments were performed with a Perkin-Elmer DMA 7e instrument (Norwalk, CT). The mode of deformation applied was the three-point bending system, and the measurements were performed via tension control, where a static force was applied as a percentage of the dynamic force. The amplitude was controlled at a fixed set point throughout the experiment and its magnitude and phase angle were recorded. The storage modulus (E'), loss modulus (E''), and the tan δ curves versus temperature were then evaluated.

The mean dimensions of the sample plaques were 2 × 4 × 15 mm. The temperature range varied from −170°C up to the melting temperature of the polymers, and the measurements were carried out at four fixed frequencies: 0.2, 1, 10, and 50 Hz.

Tensile measurements were performed with an Instron 1121 type tester (Bucks, England) at room temperature. The specimens were 30 mm in gauge length, and the applied crosshead speed was 10 mm/min. Tensile engineering stress–strain curves were then obtained up to the breaking point.

RESULTS AND DISCUSSION

From DMA experiments, the storage modulus (E'), loss modulus (E''), and tan δ values at a fixed frequency versus temperature were evaluated. The β and γ transitions were examined in respect to their peak values and the peak temperature for E'' and tan δ. These results are summarized in Table III for the frequency of 1 Hz. At higher frequencies, these peak values became slightly higher. Figure 1 demonstrates the storage modulus curves of the materials tested at a frequency of 1 Hz. Starting from −170°C, the first change in the slope, related to the γ transition, took place at −130°C. This transition was attributed to the motions of CH_2 units in the amorphous region.[11,12] The temperature region of the β transition appeared around −40°C, and as it has been reported,[13] the β transition is related to the segmental motions of dis-

TABLE II
Crystallinity and Melting Points of Ethylene Copolymers

Sample type	Melting point (°C)	Heat of fusion (J/g)	Crystallinity (%)
M_1	125	96.30	33.20
M_2	118.06	101.06	34.84

TABLE III
DMA Results of Ethylene Copolymers

	Tan δ		Tan δ (peak height)		E''		E'' (peak height; 10^8 Pa)	
			Transition				Transition	
Sample type	T_β (°C)	T_γ (°C)	β	γ	T_β (°C)	T_γ (°C)	β	γ
M_1	−22	−124	0.07	0.067	−31.17	−139.76	0.82	2.08
M_2	−20	−125	0.08	0.075	−31.78	−134	0.97	1.986

T_β: peak temperature of β-transition.
T_γ: peak temperature of γ-transition.

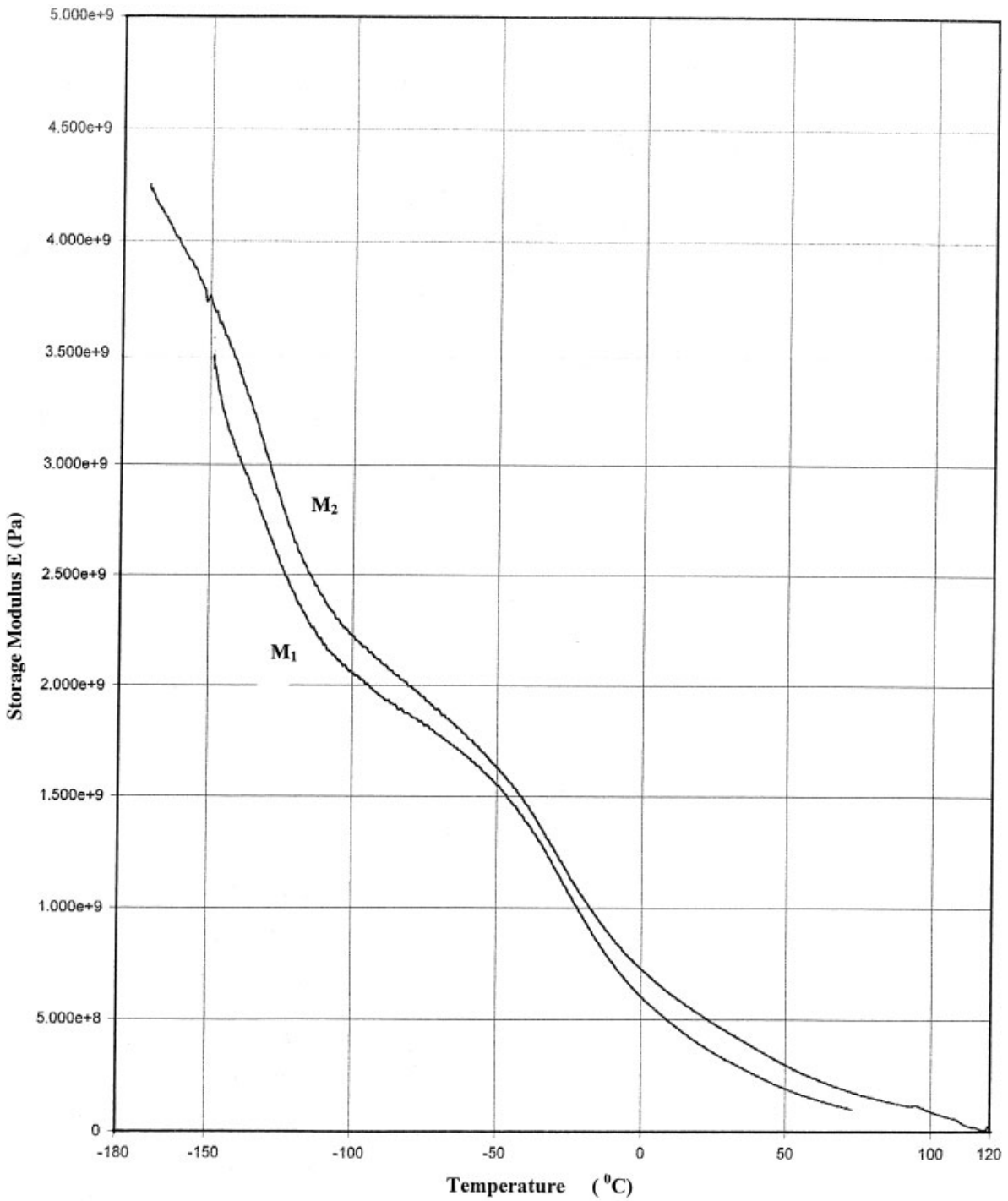

Figure 1 Storage modulus versus temperature at 1 Hz for samples M_1 and M_2.

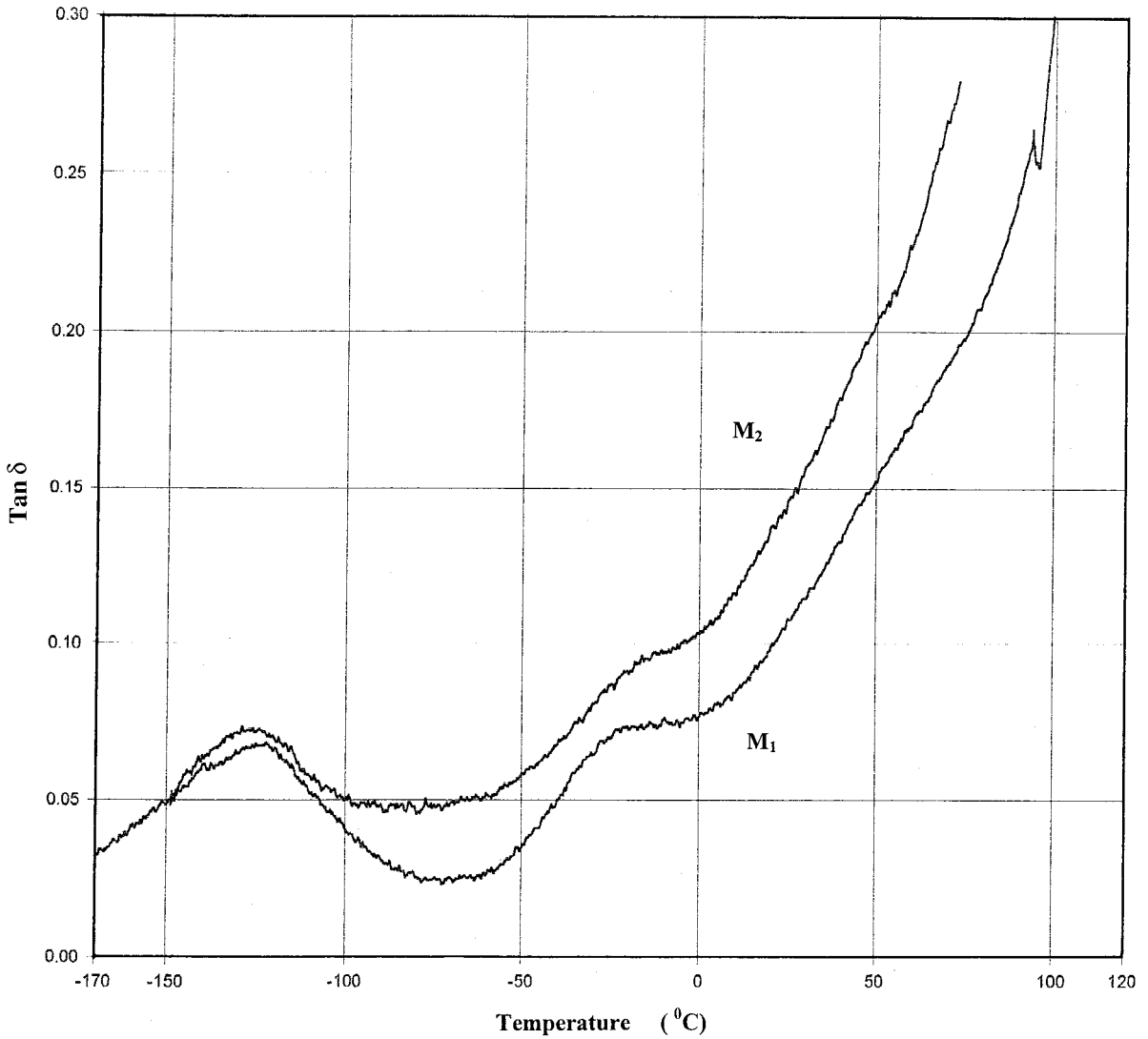

Figure 2 Tan δ versus temperature at 1 Hz for samples M_1 and M_2.

ordered chains located in interfacial region associated with lamellar crystallites.

The storage modulus of the M_1 sample was always higher than that of the M_2 sample, exhibiting the influence of micromorphology on DMA results. This trend revealed the fact that samples with lower comonomer content and better quality of crystallinity exhibited higher values of storage modulus. From the tan δ versus temperature curves presented in Figure 2, the β and γ relaxation regions of the samples can be studied. The storage modulus versus temperature data at four different frequencies, namely, 0.2, 1, 10, and 50 Hz, are presented in Figures 3 and 4 for samples M_1 and M_2, respectively. We subsequently rearranged these data by a standard time–temperature superposition principle to obtain the master curves shown in Figure 5, with respect to $\log(\omega a_T)$, where a_T is the shift factor and ω is the frequency. An analogous procedure for semicrystalline materials was followed in ref. 14. For the plotting of master curves, room temperature (20°C) was selected as a reference, due to the fact that, as is shown later, these data were related to the stress–strain results, also obtained at room temperature. To evaluate $E(t)$ as function of time, from the experimental data, the following procedure was followed: The experimental data of the storage modulus were expressed in a logarithmic time timescale (through the inversion of the initial frequency scale) and were fitted with a seventh-degree polynomial function. The derivative of this expression is the relaxation time spectrum (H) when the Alfrey approximation is considered:[15]

$$H(\tau) = -\left[\frac{dE(t)}{d\ln t}\right]_{t=\tau}.$$

where t is the time and τ is the relaxation time. The relaxation spectrum versus time in a logarithmic scale

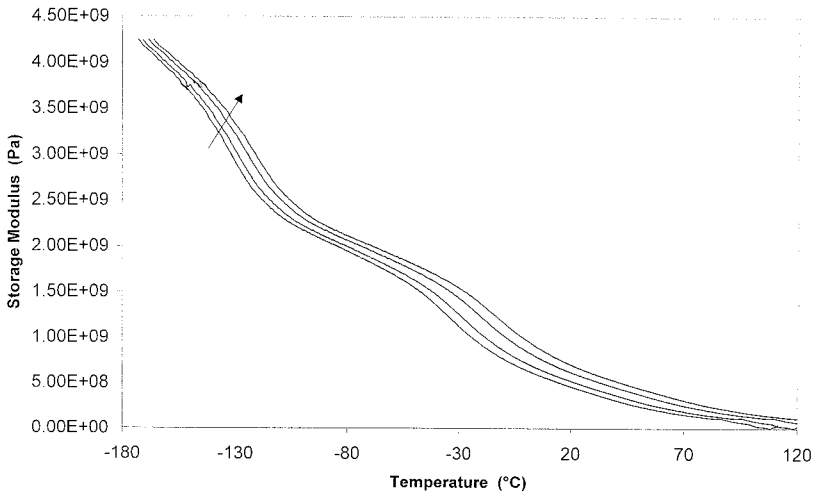

Figure 3 Storage modulus versus temperature for sample M_1 at four fixed frequencies: 0.2, 1, 10, and 50 Hz.

was obtained and is shown in Figure 6. Both types of materials exhibited two main regions of local maxima in their relaxation spectra but in rather different positions along the logarithmic timescale and with different intensities. The observed differences in the relaxation spectra, which are fundamental viscoelastic functions, reflected the corresponding differences in the micromorphology of the two types of materials, which finally affected their tensile behaviors.

Furthermore, by integrating the relaxation spectrum function, according to the previous equation, we were able to construct an approximate function of $E(t)$ as a function of time, applying the method of interpolation, with the software Mathematica.[16] Then, the modulus relaxation function of the materials in respect to time was plotted versus a conventional timescale (see Fig. 7). Both curves were of the same shape, whereas the values of sample M_1 were higher. The previously mentioned procedure consisted of an empirical method for the evaluation of $E(t)$ as a function of time, starting from DMA experiments. It is important to mention here that through this procedure, the values of $E(t)$ could be evaluated at extremely low times. Hereafter, this function can be treated as a material property and correlated with the material's macroscopic behavior.

However, engineering tensile stress–strain curves were obtained and are presented in Figure 8. Both curves exhibited the main features of the inelastic behavior of polymers, namely, the initial viscoelastic part, the stress peak, and the subsequent strain softening, followed by cold drawing and strain hardening up to the breaking point. More specifically, the yielding of semicrystalline polymers is mainly attributed to the breakage of large crystallites, whereas strain softening is strongly related to inhomogeneous deformation distribution. Thereafter, cold drawing took place, due to the relative slippage of macromolecular chains, whereas at higher strains, an intense strain hardening occurred

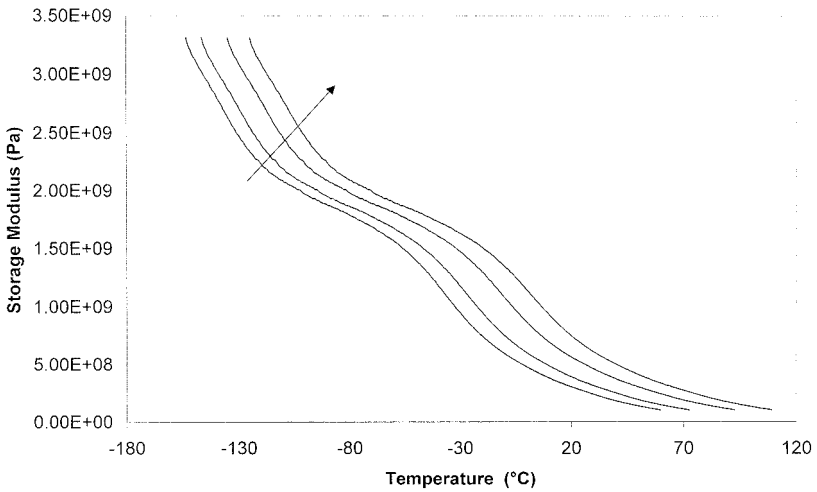

Figure 4 Storage modulus versus temperature for sample M_2 at four fixed frequencies: 0.2, 1, 10, and 50 Hz.

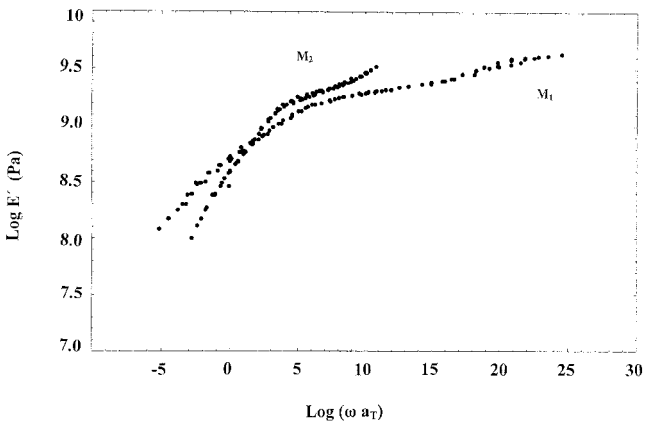

Figure 5 Master curves of storage modulus in respect to logarithmic frequency for samples M_1 and M_2 at a reference temperature of 20°C.

by the stretching of tie molecules. It is obvious from these results that the higher tensile properties of sample M_1 arose from its higher density (lower comonomer content) but mainly from the better quality of crystallites it might have had (higher melting point) compared with sample M_2.

Constitutive analysis

When one makes the assumption that the stress–strain behavior of the glassy state follows a viscoelastic path at small strains, the relation between stress and strain can be described by a single integral constitutive equation as follows:

$$\sigma = \int_0^t E(t - t') \frac{de}{dt'} dt' \qquad (1)$$

where σ is the stress, t is the upper limit of integration, t' is the integration variable, $E(t)$ is the relaxation modulus function and e is the strain. The application of the Boltzmann superposition principle was considered to be valid when we considered that at small strains before yielding, linear viscoelastic response takes place. After this stage however, plastic deformation is developed.

To describe the yield and postyield behavior after the initial viscoelastic path, we assumed that at this stage, the plastic path prevails. Therefore, there was a need to consider a suitable kinematic formulation separating the total deformation into plastic and viscoelastic parts. Such an approach, widely used by many authors,[17–20] assumes that the total deformation gradient tensor (F) separates multiplicatively into an elastic part (F_e) and a plastic part (F_p), such that

$$F = F_e F_p \qquad (2)$$

This approach was applied earlier for the yield and postyield deformation behavior of polymers by Boyce et al..[21] Among many treatments, we selected an approach developed by Rubin.[22,23] Rubin's main idea was to calculate the elastic part of strain developed during deformation procedure, through an evolution equation of a vector triad ($\mathbf{m}_i$) that is introduced to model the orientation and elastic deformation of the average atomic lattice.

Rubin's work mainly concerned with the physics of plastic flow of crystalline metals, was proved to describe successfully plastic deformation of semicrystalline and amorphous polymers as well.[24,25]

In our case, we assumed that $\mathbf{m}_i$ followed the deformation of an elementary material volume respon-

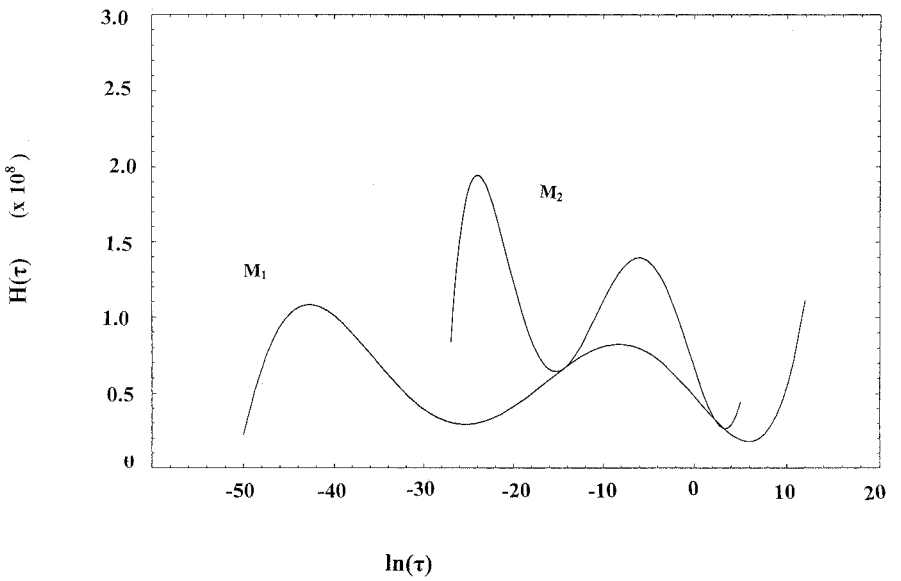

Figure 6 Relaxation time spectra in respect to the logarithmic timescale for samples M_1 and M_2.

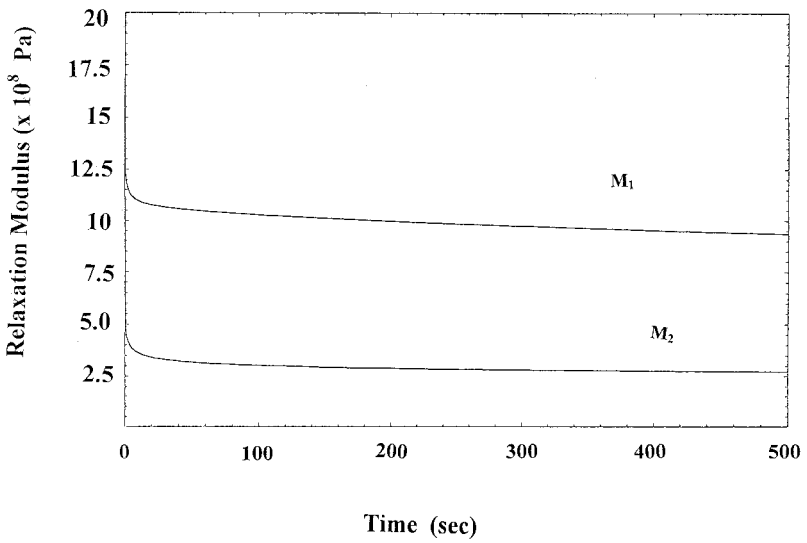

Figure 7 Function of $E(t)$ with respect to time for samples M_1 and M_2.

sible for the viscoelastic behavior of the material. The evolution equation of $\mathbf{m}_i$ is then given by the following equation:

$$\dot{\mathbf{m}}_i = L_m \mathbf{m}_i \tag{3}$$

where

$$L_m = L - L_p \tag{4}$$

where L and L_p are the velocity gradient tensors of total and plastic deformation, respectively.

In the case of uniaxial loading, only the symmetric parts D and D_p of these tensors are taken into account, so that

$$L = D, \qquad L_p = D_p \tag{5}$$

When we consider a fixed rectangular Cartesian base vector $\mathbf{e}_i$ parallel to $\mathbf{m}_i$, we have

$$\mathbf{m}_1 = \lambda_1 \mathbf{e}_1, \qquad \mathbf{m}_2 = \lambda_2 \mathbf{e}_2, \qquad \mathbf{m}_3 = \lambda_3 \mathbf{e}_3 \tag{6}$$

where λ_1, λ_2, and λ_3 are the stretch ratios of the viscoelastically deformed unit, with initial values equal

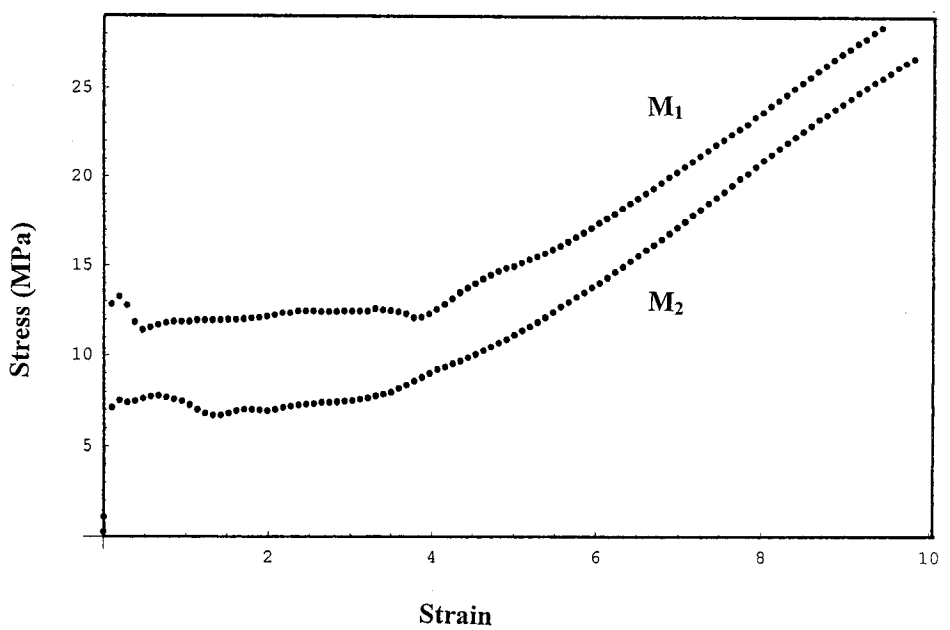

Figure 8 Experimental engineering tensile stress–strain curves for samples M_1 and M_2.

to unity. For uniaxial loading in the $\mathbf{e}_1$ direction, one can take $\lambda_2 = \lambda_3 = \lambda$. It is also convenient to define distortional measures $\mathbf{m}_i'$ of the elementary volume by the following formula:

$$\mathbf{m}_i' = J_m^{-(1/3)}\mathbf{m}_i \tag{7}$$

where J_m is the elementary volume and is equal to $\lambda_1\lambda_2\lambda_3$. The vectors $\mathbf{m}_i'$ can, therefore, be written as

$$\mathbf{m}_1' = a_m\mathbf{e}_1, \qquad \mathbf{m}_2' = \frac{1}{\sqrt{a_m}}\mathbf{e}_2, \qquad \mathbf{m}_3' = \frac{1}{\sqrt{a_m}}\mathbf{e}_3 \tag{8}$$

where a_m is the stretch ratio per cubic root of J_m.

In the content of these definitions, the velocity gradient tensor of the total deformation is specified by the form

$$\mathbf{L} = \begin{bmatrix} \dfrac{\dot{a}}{a} & 0 & 0 \\ 0 & \dfrac{\dot{b}}{b} & 0 \\ 0 & 0 & \dfrac{\dot{c}}{c} \end{bmatrix} \tag{9}$$

where a, b, and c represent the stretches of material line elements in the coordinate directions $\mathbf{e}_i$ with initial conditions $a(0) = b(0) = c(0) = 1$.

The symmetric part of the plastic velocity gradient D_p was written by Rubin[23] as an associated flow rule:

$$D_p = \Gamma_p\bar{D}_p \tag{10}$$

where the direction of $\overline{D}_p$ for plastically isotropic response is specified by the deviatoric portion of the driving stress tensor[23] and Γ_p is a nonnegative function expressing the rate of plastic deformation and needs to be specified.

For the case of uniaxial deformation, Rubin, solving the previous equations, extracted the following expression for the time evolution of the normalized stretch ratio (a_m) of volume element, which is subjected to the large imposed deformation

$$\frac{\dot{a}_m}{a_m} = \left[\frac{1 + \dfrac{1-2\nu}{2(1+\nu)}\left(\dfrac{a_m^3 - 1}{a_m}\right)}{1 + \dfrac{1-2\nu}{6(1+\nu)}\left(\dfrac{5a_m^3 - 2}{a_m}\right)}\right] \times \left[\frac{\dot{a}}{a} - \frac{\Gamma_p}{18}\left(\frac{a_m^3 - 1}{a_m^3}\right)(4a_m^3 + 2)\right] \tag{11}$$

with the initial condition $a_m(0) = 1$ and the Poisson ratio (ν) is equal to 0.3.

The quantity Γ_p, expressing the rate of plastic deformation, has been modeled in previous works,[9,25] where it was assumed that during deformation, strain is accumulated around specific regions inhomogeneously, following a normal distribution density. Integrating this distribution, we obtained the rate of plastic deformation as follows:

$$\Gamma_p = \frac{\dot{a}}{a(a_m^y - 1)}\frac{1}{s\sqrt{\pi}}\int_1^a e^{-(1/2)(a_i - \mu/s)^2}\,da_i \tag{12}$$

where $\dot{a}$ is the imposed deformation rate and a_m^y is the stretch ratio where yield takes place. The limits of integration are expressed in respect to the stretch ratio a. μ is the mean value of the probability density and is taken to be the stretch ratio a_m^y where yield occurs. The standard deviation s is a fitting parameter. When eqs. (11) and (12) are combined, the viscoelastic stretch ratio (a_m) and its time derivative ($\dot{a}_m$) can be evaluated at every stage of deformation. These values of $\dot{a}_m$ were thereafter introduced into eq. (1), replacing the strain rate (de/dt') and leading to stress evaluation.

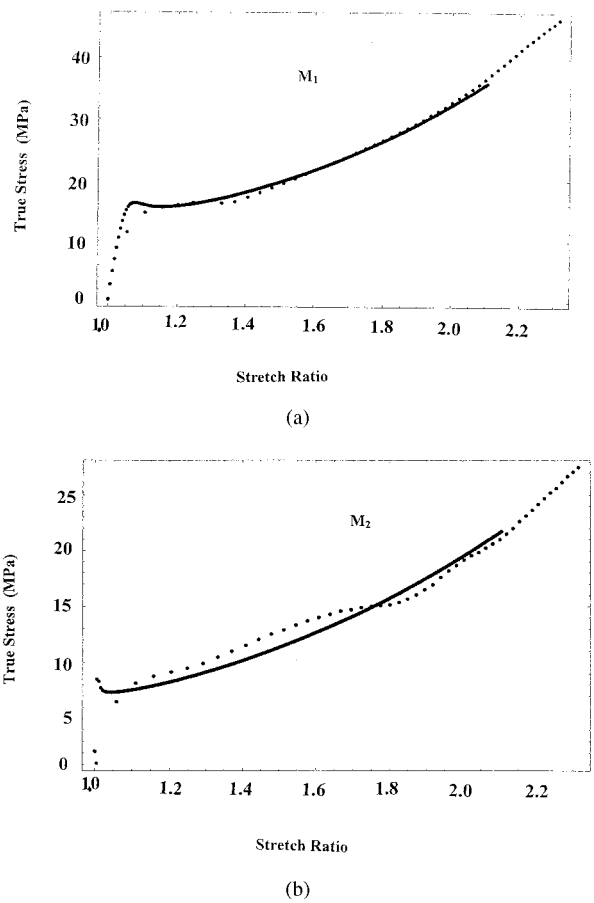

Figure 9 Tensile stress–stretch ratio curves at a crosshead speed of 10 mm/min for samples (a) M_1 and (b) M_2: (○) experimental data and (—) theoretical predictions.

As shown in the experimental results of the stress–strain curves, a strain hardening took place at high values of deformation. To obtain the complete calculation of stress, including this stage, a supplementary term (σ_h) for stress should be taken into account, due to the entropic hardening,[26] as an additive term to the constitutive eq. (1). This additional stress is given by

$$\sigma_h = G_p \frac{\sqrt{N}}{3}\left[a_{p_1} L^{-1}\left(\frac{a_{p_1}}{\sqrt{N}}\right) - \frac{1}{3}\sum_{j=1}^{3} a_{p_j} L^{-1}\left(\frac{a_{p_j}}{\sqrt{N}}\right)\right] \quad (13)$$

where a_{pi} is the stretch ratios in the three principal directions with $a_{p1} = 1 + a - a_m$, and $a_{p2} = a_{p3} = 1/(a_{p1})^{0.5}$; N is the equivalent number of rigid links between entanglements (equal to 20); and G_p is the strain hardening modulus (equal to 5 MPa). The G_p value is obtained from the slope of the stress–strain curve in the region of large deformations, where strain hardening takes place. Because G_p expresses a shear modulus, it is equal to the slope value divided by 3. The value of N was estimated from the best fit of the experimental stress–strain curves.

Integration in eqs. (1), (11), and (12) was made numerically with small time steps until a high convergence was obtained. Following this procedure, we could describe the stress–strain response of the materials in detail. The theoretical results in respect to the experimental data are shown in Figure 9 (at a value of stretch ratio up to 2.2), where a good approximation was testified for the entire shape of the experimental curves. The experimental curves of Figure 9 were plotted in terms of the true stress–strain data in respect to the experimental results plotted in Figure 8. It is important to mention here once again that $E(t)$ was evaluated from dynamic mechanical tests, and through this analysis, it was possible to predict satisfactorily the total stress–strain behavior in a quasistatic tensile experiment.

CONCLUSIONS

In this work, we examined two types of metallocene ethylene–*a*-olefin copolymers with some essential differences in their micromorphology that affected their macroscopic behavior.

The viscoelastic behavior of the materials was studied in a wide temperature range at four different frequencies in terms of DMA, and the experimental curves of $E(t)$ were obtained. By this method, values of $E(t)$ at extremely low values of time were available. Hereafter, this function satisfactorily predicted the stress–strain response of the material in the initially linear viscoelastic region in terms of a single integral constitutive equation without the requirement for any additional model parameters. For higher values of deformation, where plastic strain was enhanced, a plasticity theory of separating the plastic and viscoelastic part of strain was applied, for a complete description of the stress–strain behavior.

References

1. Rendell, R. W.; Ngai, K. L.; Fong, G. R.; Yee, A. F.; Bankert, R. J. Polym Eng Sci 1987, 27, 2.
2. Tervoort, T. A.; Klompen, E. T. J.; Govaert, L. E. J Rheol 1996, 40, 5.
3. Bernstein, B.; Shokooh, A. J Rheol 1980, 24(2), 189.
4. McKenna, G. B.; Zapas, L. J. Soc Rheol 1980, 24(4), 367.
5. McKenna, G. B. J Rheol 1979, 23(2), 151.
6. Wu, P. D.; van der Giessen, E. J Mech Phys Sol 1993, 41, 427.
7. Knauss, W.; Emri, R. Presented at the ASME Winter Meeting, 1989.
8. Hasan, O. A.; Boyce, M. C. Polym Eng Sci 1995, 35, 331.
9. Spathis, G.; Kontou, E. Polym Eng Sci 2001, 41, 1337.
10. Brady, J. M.; Thomas, E. L. J Polym Sci Part B: Polym Phys 1988, 26, 2385.
11. Popli, R.; Glotin, M.; Mandelkern, L. J. J Polym Sci Polym Phys Ed 1984, 22, 407.
12. McCrum, N. G.; Read, B. E.; Williams, G. Anelastic and Dielectric Effects in Polymeric Solids; Dover: New York, 1991.
13. Starck, P. Eur Polym J 1997, 33, 339.
14. Pegoretti, A.; Guardini, A.; Migliaresi, C.; Ricco, T. J Appl Polym Sci 2000, 78, 1664.
15. Ferry, J. D. Viscoelastic Properties of Polymers, 2nd ed.; Wiley: New York, 1970.
16. Wolfram, S. The Mathematica Book, 4th ed.; Wolfram Media/Cambridge University Press: New York, 1999.
17. Lee, E. H.; Liu, D. T. J Appl Phys 1967, 38, 19.
18. Lee, E. H. J Appl Mech 1969, 36, 1.
19. Mandel, J. Int J Solids Struct 1973, 9, 725.
20. Dafalias, Y. F. Plasticity Today; Elsevier: Amsterdam, 1985; p 135.
21. Boyce, M. C.; Parks, M.; Argon, A. S. Mech Mater 1988, 7(1), 15.
22. Rubin, M. B. Int J Solids Struct 1994, 31, 2635.
23. Rubin, M. B. Int J Solids Struct 1994, 31, 2615.
24. Spathis, G.; Kontou, E. Polymer, 1998, 39, 135.
25. Spathis, G.; Kontou, E. J Appl Polym Sci, to appear.
26. James H. M.; Guth, E. J Polym Sci 1943, 11, 455.